

Analysis of Needle–Tissue Friction during Vibration-Assisted Needle Insertion

Iman Khalaji, Mostafa Hadavand, Ali Asadian, Rajni V. Patel*, and Michael D. Naish

Abstract—In this paper, a vibration-assisted needle insertion technique has been proposed in order to reduce needle–tissue friction. The LuGre friction model was employed as a basis for the current study and the model was extended and analyzed to include the impact of high-frequency vibration on translational friction. Experiments were conducted to evaluate the role of insertion speed as well as vibration frequency on frictional effects. In the experiments conducted, an 18 GA brachytherapy needle was vibrated and inserted into an *ex-vivo* soft tissue sample using a pair of amplified piezoelectric actuators. Analysis demonstrates that the translational friction can be reduced by introducing a vibratory low-amplitude motion onto a regular insertion profile, which is usually performed at a constant rate.

I. INTRODUCTION

The use of flexible needles in percutaneous interventions such as biopsy, drug delivery, brachytherapy, neurosurgery and tumor ablation has attracted many researchers. Particularly when target points are not directly accessible inside soft tissue, this type of intervention is more appealing. Needle tip misplacement can, however, degrade the effectiveness of the therapy or diagnosis. In this context, robotics-assisted needle intervention has been proposed as a solution to enhance targeting accuracy [1]. Nonetheless, targeting inaccuracies still occur due to effects such as (1) target movement as a result of soft tissue deformation, (2) needle bending due to the complex nature of needle–tissue interaction, and (3) inhomogeneity and anisotropy of real organic tissue [2].

In order to increase targeting accuracy, the complex interaction between the needle and soft tissue has to be fully investigated. Okamura et al. [3] were the first to define needle insertion as a three-phase procedure, namely pre-puncture,

post-puncture and retraction or needle withdrawal. While viscoelastic behavior dominates the pre-puncture phase, the combined effects of cutting force, friction and tissue relaxation govern the post-puncture step. As an analytical study in this area, Mahvash and Dupont [4] proposed a fast needle insertion technique as a means of decreasing pre-puncture force and needle deflection, thereby improving positioning accuracy. They considered the role of insertion rate and linked it to the interaction forces. Nevertheless, the safety of such a “needle shooting” procedure for living tissue particularly at close proximity to vital organs such as the heart and lungs is questionable.

As a major force component in needle–tissue interaction, translational friction deserves further study. It is believed that by controlling or at least minimizing frictional effects, soft tissue deformation can be significantly reduced, which in turn would result in better targeting accuracy for needle-based interventional procedures. This idea is the main motivation for the current study.

II. RELATED WORK

Velocity modulation during needle insertion is an approach that has been proposed in research papers in order to guide a flexible needle or minimize tissue deformation [5]. In the context of control, Minhas et al. [6] developed a duty-cycled spinning technique to adjust the needle trajectory and steer it into soft tissue. From force analysis perspective, high-frequency translational oscillation and rotational drilling were reported to reduce needle–tissue interaction forces as well as tissue deformation [7], [8]. Likewise, reduced tissue indentation and frictional forces were reported in [9] when using a low frequency rotational motion. Nonetheless, needle spinning may induce tissue damage due to any minor defect in needle straightness, off-centric rotation or macro-structural defects at the needle tip as a result of imperfect machining. In order to address this issue, post-revolving the needle was shown to have the same benefit and to reduce targeting error [10].

Shin-ei et al. [11] were the first to report a reduction in needle insertion force by inducing mechanical vibration into a hypodermic needle. Using multilayer piezoelectric elements, the needle, which was forced to vibrate laterally in the frequency range up to 10 kHz, was inserted into swine muscle tissue. A maximum reduction of 69% in interaction force was reported in their work [11]. However, it is unclear what vibration amplitude and insertion velocity were used to conduct the experiments. Muralidharan [12] also investigated the effect of longitudinal vibration in terms of its amplitude

The authors are with Canadian Surgical Technologies and Advanced Robotics (CSTAR), Lawson Health Research Institute, London, Canada. I. Khalaji is with the Department of Mechanical and Materials Engineering, Western University (The University of Western Ontario). M. Hadavand is with the Biomedical Engineering Graduate Program, Western University. A. Asadian is with the Department of Electrical and Computer Engineering, Western University. R.V. Patel (*Project Leader) is with the Department of Electrical and Computer Engineering and the Department of Surgery, Western University. M.D. Naish is also with the Department of Mechanical and Materials Engineering and the Department of Electrical and Computer Engineering, Western University (emails: ikhalaji@uwo.ca, mhadavand@uwo.ca, aasadian@uwo.ca, rypatel@uwo.ca, mnaish@uwo.ca).

This research is supported by the Natural Sciences and Engineering Research Council (NSERC) of Canada under grants RGPIN-1345 (R.V. Patel), and 312383 (M.D. Naish); and by an NSERC-CIHR (Canadian Institutes for Health Research) Collaborative Health Research Projects Grant #398137-2011 (PI: R.V. Patel); and by infrastructure grants from the Canada Foundation for Innovation awarded to CSTAR and to Western University. Financial support for I. Khalaji, M. Hadavand, and A. Asadian has also been provided through an NSERC Collaborative Research and Training Experience (CREATE) program grant #371322-2009 in Computer-Assisted Medical Interventions (CAMI). I. Khalaji and A. Asadian have also been supported by Ontario Graduate Scholarships (OGS).

and frequency on the penetration force (in both soft tissue and tissue surrogate) using a permanent magnet shaker. The reported results support a reduction in the penetration force of 2 to 3 times when using a higher vibration amplitude and frequency. However, no statistical interaction analysis was provided in this study.

Inspired by motions during a mosquito bite, it is believed that vibration-assisted needle insertion minimizes pain [12]. If true, this technique can potentially enhance needle-based interventions such as bone biopsy [13] by lowering interaction forces and increasing accuracy. In the current study, a mathematical analysis is performed to justify why in general during vibration-assisted needle insertion, the friction force is reduced. The presented model, which exploits the LuGre friction model [14], establishes an explicit relationship between the vibration parameters including motion amplitude and frequency and the force magnitude. Moreover, experiments performed on soft tissue samples serve to validate the model.

The rest of this paper is organized as follows. Section III explains the role of vibration on frictional effects using the LuGre model. Section IV describes the experimental evaluation while Section V presents conclusions and suggestions for future work.

III. MATHEMATICAL ANALYSIS OF NEEDLE-TISSUE FRICTION USING VIBRATION

Asadian et al. [15] developed a distributed version of the LuGre friction model [14] along the inserted portion of a needle to model friction effects during needle insertion. This physically-inspired model is based on the bending of spring-like bristle elements that exist at the microscopic level of moving surfaces. As a basis for the current analysis, the LuGre structure [15] is briefly reviewed here.

Considering $z(\zeta, t)$ as the model's internal state or the deflection of the bristle elements located at the point ζ at a certain time t , the distributed LuGre model can be written as [14], [15]:

$$\begin{cases} \frac{dz}{dt}(\zeta, t) = v - \frac{\sigma_0|v|}{g(v)}z \\ F_{\text{friction}}(t) = \int_0^{L(t)} dF(\zeta, t) \end{cases} \quad (1)$$

$$g(v) = \mu_c + (\mu_s - \mu_c)e^{-\alpha|v|}, \quad (2)$$

where v is the velocity of each differential element and $L(t)$ is the needle length that is being inserted into soft tissue at time t . Moreover,

$$dF(\zeta, t) = \left(\sigma_0 z(\zeta, t) + \sigma_1 \frac{\partial z}{\partial t}(\zeta, t) + \sigma_2 v \right) dF_n(\zeta, t), \quad (3)$$

is the differential friction force that is proportional to the differential normal force, $dF_n(\zeta, t)$ applied to the element $d\zeta$ at time t . In total, the friction force can be characterized by four static parameters, i.e., μ_c , μ_s , σ_2 and α , as well as two dynamic parameters, namely σ_0 and σ_1 . As can be seen in Fig. 1, σ_0 and σ_1 can be understood as the stiffness and damping coefficients of the microscopic elastic bristles, whereas σ_2 , μ_c and μ_s are the viscous damping, normalized Coulomb and stiction friction coefficients [15].

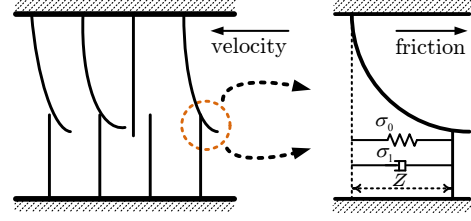


Fig. 1. Microscopic representation of irregular contact surfaces and elastic bristles whose bending gives rise to the friction force (Reproduced from [15], © Copyright IEEE, 2011).

Assuming a uniform normal force distribution along the needle and a constant patch region of needle within soft tissue, i.e., $\frac{dL}{dt} = 0$, (1) can be simplified to [15]:

$$\begin{cases} \dot{\tilde{z}} = v - \frac{\sigma_0|v|}{g(v)}\tilde{z} \\ F_{\text{friction}}(t) = F_n (\sigma_0 \tilde{z} + \sigma_1 \dot{\tilde{z}} + \sigma_2 v) \end{cases}, \quad (4)$$

where \tilde{z} is the mean friction state. Note that in the above state-space representation, all static and dynamic parameters are functions of the interaction characteristics and are independent of the insertion rate¹.

Assuming a zero initial condition, i.e., $\tilde{z}(0) = 0$, the general solution of the ordinary differential equation described in (4) is of the form:

$$\tilde{z}(t) = \frac{g(v(t))}{\sigma_0} \text{sgn}(v(t)) \left(1 - e^{-\sigma_0 \int_0^t \frac{|v(t)|}{g(v(t))} dt} \right). \quad (5)$$

A. Needle Insertion at Constant Velocity

Now consider a situation where a constant length of a needle has been inserted into a block of soft tissue, while its tip is outside the other side of the block. While the needle is being advanced toward soft tissue with a constant velocity, i.e., $v(t) = v_0$, a constant length of the needle maintains contact with soft tissue. Therefore, (5) can be further simplified as:

$$\tilde{z}(t) = \frac{g(v_0)}{\sigma_0} \text{sgn}(v_0) \left(1 - e^{-\frac{\sigma_0}{g(v_0)}|v_0|t} \right). \quad (6)$$

Inserting (6) into (4), the total friction force can be obtained as:

$$F_{\text{friction}}(t) = F_n \{ (\sigma_1 v_0 - g(v_0) \text{sgn}(v_0)) e^{-\frac{\sigma_0}{g(v_0)}|v_0|t} + g(v_0) \text{sgn}(v_0) + \sigma_2 v_0 \}. \quad (7)$$

Hence, the steady-state friction force for sufficiently large values of v_0 is:

$$F_{\text{friction,ss}} = F_n \{ \mu_c + \sigma_2 v_0 \}. \quad (8)$$

Referring to (8), for sufficiently large values of time, t , viscosity and Coulomb friction are the only components that constitute the friction force. Moreover, increasing the insertion rate makes the total friction force bigger due to the viscous term. Roughly speaking, at very high velocities, viscosity totally dominates the Coulomb friction term.

¹In general, σ_2 is a function of v and decreases as the velocity increases. In this section, σ_2 is, however, assumed to be constant.

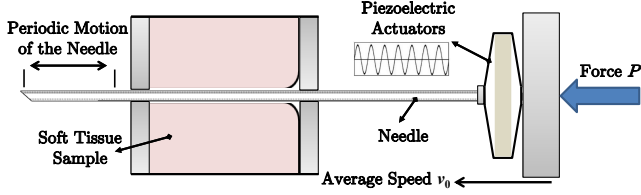


Fig. 2. Schematic demonstration of the proposed needle insertion setup.

B. Vibration-Assisted Needle Insertion

Now, suppose that a needle is vibrated longitudinally while it is being inserted into soft tissue. Investigation of the effect of such velocity modulation on the friction force is described in this section. While a few researchers have reported a reduction in the friction force due to a modulated velocity [7], to the best of the authors' knowledge, no one has ever systematically studied the effect of vibration and velocity modulation on the friction force.

As illustrated in Fig. 2, suppose that a vibration generator has been attached to the distal end of a needle. The generator applies a longitudinal sinusoidal force to the needle structure. In order to perform an insertion procedure, the whole unit, including the needle and the vibration generator, is moved with an average speed v_0 . Also, assume that the unit is subject to a static force P . Without loss of generality, consider the following functional form for the insertion velocity²:

$$v(t) = v_0 + a\omega \cos(\omega t), \quad (9)$$

where a and ω are the amplitude and frequency of vibration. By substitution of (9) into (5), the mean friction state can be obtained as:

$$\begin{aligned} \bar{z}(t) &= \frac{g(v_0 + a\omega \cos(\omega t))}{\sigma_0} \operatorname{sgn}(v_0 + a\omega \cos(\omega t)) \\ &\times \left(1 - e^{-\sigma_0 \int_0^t \frac{|v(t)|}{g(v(t))} dt} \right). \end{aligned} \quad (10)$$

Let us define $u(t) = \int_0^t \frac{|v(t)|}{g(v(t))} dt$. For sufficiently large values of time t , u becomes very large since it is a nondecreasing function with respect to time, i.e., $u'(t) = \frac{|v(t)|}{g(v(t))} \geq 0$. Therefore, the mean deflection state in (10) becomes:

$$\bar{z}(t) = \frac{g(v_0 + a\omega \cos(\omega t))}{\sigma_0} \operatorname{sgn}(v_0 + a\omega \cos(\omega t)). \quad (11)$$

Using (11) in (4), the instantaneous friction force can then be approximated as a function of $v(t)$. Due to the periodic nature of the insertion profile, $F_{\text{friction}}(t)$ is, in fact, a periodic function with a period of $T = 2\pi/\omega$. Considering this fact, and using the theory of momentum [16], the constant force P can be expressed as:

$$P = \frac{1}{T} \int_{t_1}^{t_1+T} F_{\text{friction}}(t) dt. \quad (12)$$

²Since needle is a long hollow tube, its first few lateral natural frequencies are much smaller than the first longitudinal resonance frequency. It can be assumed that the vibration source will not excite the needle near its natural frequencies to avoid lateral resonances. Lateral resonance can also be avoided by imposing one or two lateral nodes along the vibrating needle.

Therefore, considering (12) and (4), we have

$$\begin{aligned} P &= \frac{1}{T} \int_{t_1}^{t_1+T} F_n (\sigma_0 \bar{z} + \sigma_1 \dot{\bar{z}} + \sigma_2 v) dt \\ &= \frac{F_n}{T} \left(\underbrace{\sigma_0 \int_{t_1}^{t_1+T} \bar{z} dt}_{\text{I}} + \underbrace{\sigma_1 \int_{t_1}^{t_1+T} \dot{\bar{z}} dt}_{\text{II}} + \underbrace{\sigma_2 \int_{t_1}^{t_1+T} v dt}_{\text{III}} \right), \end{aligned} \quad (13)$$

where \bar{z} is obtained from (11).

The third integral (III) in (13) can be rewritten as:

$$\int_{t_1}^{t_1+T} v dt = \int_{t_1}^{t_1+T} (v_0 + a\omega \cos(\omega t)) dt = v_0 T. \quad (14)$$

In order to obtain the second integral (II) in (13), (11) is used to rewrite the integrand, $\dot{\bar{z}}$:

$$\dot{\bar{z}} = \frac{1}{\sigma_0} \frac{\partial g(v)}{\partial v} v'(t) \operatorname{sgn}(v(t)) = \frac{-\alpha(\mu_s - \mu_c)}{\sigma_0} v'(t) e^{-\alpha|v(t)|}. \quad (15)$$

According to (15), $\dot{\bar{z}}$ is a continuous function over $[t_1, t_1 + T]$, thus:

$$\int_{t_1}^{t_1+T} \dot{\bar{z}} dt = \bar{z}(t_1 + T) - \bar{z}(t_1) = 0. \quad (16)$$

Note that to derive (16), the periodicity of \bar{z} with period T is taken into account.

Using (11), the first integral (I) in (13) can be simplified as:

$$\begin{aligned} \int_{t_1}^{t_1+T} \bar{z} dt &= \int_{t_1}^{t_1+T} \frac{g(v(t))}{\sigma_0} \operatorname{sgn}(v(t)) dt \\ &= \frac{\mu_c}{\sigma_0} \int_{t_1}^{t_1+T} \operatorname{sgn}(v_0 + a\omega \cos(\omega t)) dt \\ &+ \frac{\mu_s - \mu_c}{\sigma_0} \int_{t_1}^{t_1+T} e^{-\alpha|v_0 + a\omega \cos(\omega t)|} \operatorname{sgn}(v_0 + a\omega \cos(\omega t)) dt. \end{aligned} \quad (17)$$

In order to simplify (17), let us assume two special cases:

- If $|v_0| > a\omega$, $v(t) = v_0 + a\omega \cos(\omega t)$ will be a single-sign function (either positive or negative) and therefore, (17) can be obtained as:

$$\begin{aligned} \int_{t_1}^{t_1+T} \bar{z} dt &= \frac{T}{\sigma_0} \{ \mu_c + (\mu_s - \mu_c) e^{-\alpha|v_0|} I_0(\alpha a\omega) \} \\ &\times \operatorname{sgn}(v_0), \end{aligned} \quad (18)$$

where $I_0(x)$ is the modified Bessel function of the first kind and zero order at x . Note that, $I_0(x) \geq 1$ for $\forall x$.

- If $|v_0| < a\omega$, after a few manipulations, (17) can be simplified as:

$$\int_{t_1}^{t_1+T} \tilde{z} dt = \frac{\mu_c}{\sigma_0} \int_{t_1}^{t_1+T} \text{sgn}(v(t)) dt + \text{sgn}(v_0) \frac{\mu_s - \mu_c}{\sigma_0} \times \left(\int_{t_1}^{t_1+T} e^{\frac{-\alpha v(t)}{\text{sgn}(v_0)}} dt - 2 \int_{t_1+t_1^*}^{t_1+t_2^*} \cosh(\alpha v(t)) dt \right), \quad (19)$$

where t_1^* and t_2^* denotes the moments when the insertion velocity, $v(t)$, changes its sign:

$$\begin{aligned} \tau_1 = \omega t_1^* &= \arccos\left(-\frac{v_0}{a\omega}\right) = \frac{\pi}{2} + \arcsin\left(\frac{v_0}{a\omega}\right) \\ \tau_2 = \omega t_2^* &= 2\pi - \tau_1. \end{aligned} \quad (20)$$

Considering (20), (19) can be further simplified as:

$$\begin{aligned} \int_{t_1}^{t_1+T} \tilde{z} dt &= \frac{T}{\sigma_0} \text{sgn}(v_0) \left\{ \frac{2\mu_c}{\pi} \arcsin\left(\frac{v_0}{a\omega}\right) + (\mu_s - \mu_c) \right. \\ &\quad \times [e^{-\alpha|v_0|} I_0(\alpha a\omega) \\ &\quad \left. - \frac{\pi}{\omega} \int_{t_1+t_1^*}^{t_1+t_2^*} \cosh(\alpha v_0 + \alpha a\omega \cos(\omega t)) dt \right\}. \end{aligned} \quad (21)$$

Finally, using (16), (14), (18) and (21), the total friction force P in (13) is specified as follows:

- For $|v_0| > a\omega$, the total force becomes:

$$P = \overbrace{F_n \{ \mu_c + (\mu_s - \mu_c) e^{-\alpha|v_0|} I_0(\alpha a\omega) \}}^{P_{\text{Coulomb}}} \times \text{sgn}(v_0) + F_n \sigma_2 v_0. \quad (22)$$

- When $|v_0| < a\omega$, P can be obtained as:

$$\begin{aligned} P &= F_n \text{sgn}(v_0) \left\{ \frac{2\mu_c}{\pi} \arcsin\left(\frac{v_0}{a\omega}\right) + (\mu_s - \mu_c) \right. \\ &\quad \times [e^{-\alpha|v_0|} I_0(\alpha a\omega) \\ &\quad \left. - \frac{\pi}{\omega} \int_{t_1+t_1^*}^{t_1+t_2^*} \cosh(\alpha v_0 + \alpha a\omega \cos(\omega t)) dt \right\} \\ &\quad + F_n \sigma_2 v_0. \end{aligned} \quad (23)$$

Comparing (22) and (23) with (8), it is obvious that the viscous component of the total friction force, i.e., $F_n \sigma_2 v_0$, remains intact, even in the presence of vibration. The Coulomb friction force, however, changes as a vibrating needle is inserted into tissue. The dependence of the normalized static force required for the Coulomb portion, P_{Coulomb} , on the ratio of speeds, $\frac{v_0}{a\omega}$ is shown in Fig. 3. To obtain such a curve, μ_s is assumed to be an order of magnitude larger than μ_c . As seen in this graph, vibration reduces the static force required to counteract Coulomb friction when $|v_0| < a\omega$.

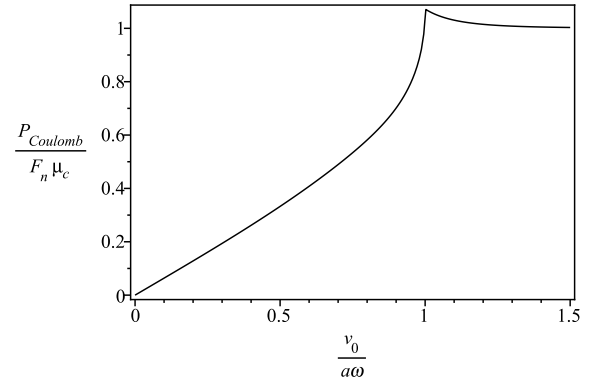


Fig. 3. Mathematical dependency of the normalized Coulomb friction force on $\frac{v_0}{a\omega}$ during vibration-assisted needle insertion.

For very small v_0 values or very large vibration speeds, i.e., $a\omega \gg |v_0|$, (23) gives:

$$P = F_n \left(\frac{2\mu_c}{\pi a\omega} + \sigma_2 \right) v_0. \quad (24)$$

Equation (24) shows how vibration-assisted insertion drives the behavior of the medium from Coulomb/viscous friction into a pure linear viscous friction with a much lower friction coefficient.

IV. INSTRUMENTATION AND EXPERIMENTAL EVALUATION

A. Experimental Setup

Experimental evaluation of the effect of vibration on needle–tissue friction was carried out using the setup shown in Fig. 4, where a vibrating needle is inserted into a soft tissue specimen using a linear motor at various speeds. The interaction forces between the needle and the tissue sample were then transferred to a desktop PC for further analysis.

The tissue sample holder was manufactured using a rapid prototyping machine and had removable side walls to facilitate needle insertion. The holder was attached to a Nano43 6-DOF force/torque sensor (ATI Industrial Automation) in order to measure the interaction forces. Two Amplified Piezoelectric Actuators (APA60SM[®], Cedrat Technologies), which were aligned side-by-side on a heavy stainless steel disk base, were employed as the vibration source unit. A 7075-T6 aluminum bar was micro-machined to attach an 18 GA stainless steel brachytherapy needle (Cook Medical) to the driving actuators (see Fig. 4). The actuator unit was subsequently mounted on top of a T-LSR300B motorized linear stage (Zaber Technologies) using another rapid-prototyped adapter. A dual-channel AFG 3022B arbitrary function generator (Tektronix) was then employed to generate sinusoidal signals whose amplitudes and frequencies were precisely controlled by the operator through a desktop computer. The generated signals were amplified using an LE 150/200-2 dual-channel analogue high-power amplifier (Piezomechanik Dr. Lutz Pickelmann GmbH), and were fed into the two piezoelectric actuators to drive the needle and its attachments at the desired amplitude and frequency.

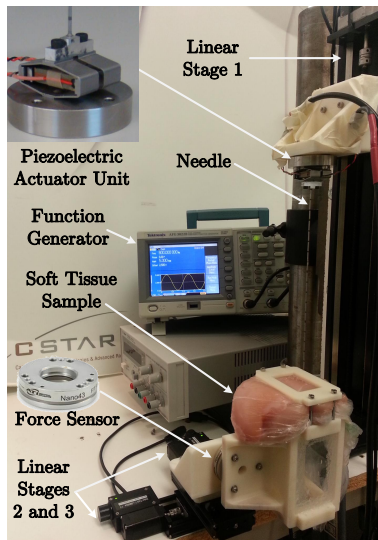


Fig. 4. Two APA60SM piezoelectric actuators were mounted on a heavy stainless steel base. An 18 GA brachytherapy needle, glued to an aluminum link bar, was vibrated longitudinally using the actuators. Linear Stage 1 performs needle insertion, while the other two linear stages facilitate tissue motion for multiple needle insertions at various locations.

B. Experimental Design

In order to assess the validity of the current analysis, an experiment was designed to measure the friction force while a constant length of the needle was inserted into a tissue sample. A stack of two-layer fresh chicken breast clamped on the holder was employed as the sample. In order to eliminate the effect of variable soft tissue thickness at various insertion locations, a preliminary insertion was made without vibration. The same hole was then used to investigate frictional effects during five consecutive insertions with various vibration frequencies. To collect each data set, the following insertion-retraction procedure was carried out:

- 1) The needle was inserted into soft tissue at a constant velocity, v_0 , with no vibration.
- 2) Once the needle had penetrated right through the sample, it was stopped for 30 seconds while vibration at a certain frequency and amplitude was started in the actuator unit.
- 3) The vibrating needle was advanced 6 cm into the tissue at velocity v_0 .
- 4) The vibrating needle was retracted 6 cm from the tissue at velocity v_0 .
- 5) The vibrating needle was again advanced 6 cm at velocity v_0 .
- 6) The vibrating needle was completely retracted from the tissue at velocity v_0 .

Following this procedure, the role of tissue pre-puncture and cutting forces during needle insertion can be assumed to have been eliminated. Therefore, it is safe to assume that friction and tissue relaxation were dominant in the resulting interaction forces.

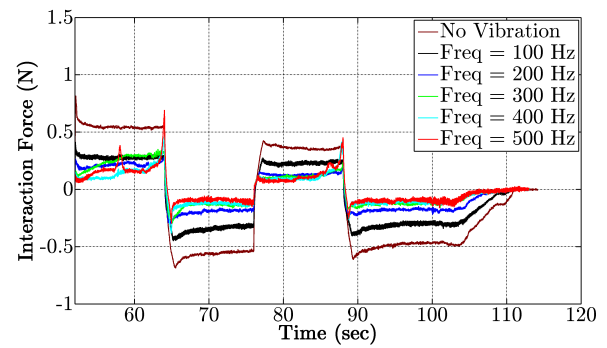


Fig. 5. Measured force values during needle insertion at various frequencies (constant insertion velocity $v_0 = 5$ mm/sec, vibration amplitude = $30 \mu\text{m}$ p-p).

C. Experimental Results

Twenty four sets of needle insertion experiments were performed on fresh chicken breast pieces using various vibration frequencies as well as insertion velocities. Tests were also performed with no vibration of the needle. Figs. 5–8 show the results of insertion at two different velocities, i.e., $v_0 = 5$ mm/sec and 10 mm/sec, into four adjacent insertion sites. The periodic insertion-retraction motion of the needle inside soft tissue can be observed as four distinct regions in the figures where the interaction forces remain almost constant until the direction of needle motion changes. As may be observed in the plots, the level of interaction force is higher for nonvibrating needle insertion, whereas it reduces as the frequency of vibration increases.

While no vibration sensor was used to measure the micron-scale vibration of the needle during the procedure, the driving voltage of the piezoelectric actuators was utilized as the determining factor to determine the vibration amplitude, a . In fact, it was assumed that both actuators produced similar vibration amplitude; hence, no nonlinear vibration mode was considered in actuating the needle. In an attempt to replicate Fig. 3 from the experimental results, the mean force values of the obtained results during insertion-retraction (Figs. 5–8), were calculated and paired with the corresponding values of $\frac{v_0}{a\omega}$ for each needle insertion procedure. The results shown in Fig. 9 indicate a good agreement between the experiments and the theoretical approach. Slight scattering of the data in this figure could be due to the fact that the needle was inserted in various sites in tissue sample, where the needle length and soft tissue properties were not identical throughout the experiments. On the other hand, inhomogeneity, nonlinear viscoelasticity, and anisotropy of chicken breast may be another reason why our empirical observations plotted in Fig. 9 do not exactly follow the expected theoretical graph shown in Fig. 3.

V. CONCLUSIONS AND FUTURE WORK

As is known, friction is a significant force component in needle–tissue interaction during percutaneous interventions. An analytical solution was presented to incorporate the impact of amplitude and frequency variation of a vibratory

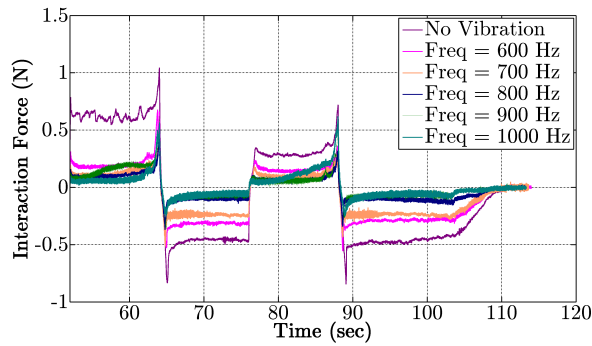


Fig. 6. Measured force values during needle insertion at various frequencies (constant insertion velocity $v_0 = 5$ mm/sec, vibration amplitude = $30 \mu\text{m}$ p-p).

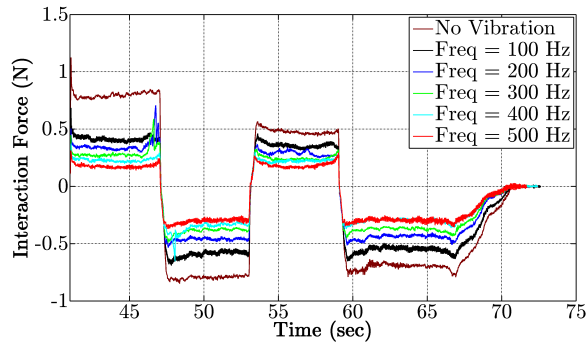


Fig. 7. Measured force values during needle insertion at various frequencies (constant insertion velocity $v_0 = 10$ mm/sec, vibration amplitude = $30 \mu\text{m}$ p-p).

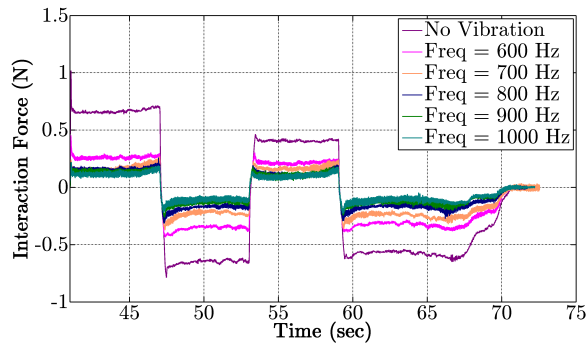


Fig. 8. Measured force values during needle insertion at various frequencies (constant insertion velocity $v_0 = 10$ mm/sec, vibration amplitude = $30 \mu\text{m}$ p-p).

insertion profile on translational friction. The analysis was based on the LuGre friction model, which has been widely discussed in the literature. The experimental results illustrate that within a certain range of the amplitudes and frequencies, the theoretical model holds true. As observed, the total friction force drops as the frequency of the vibration increases relative to the insertion velocity. By minimizing frictional effects, soft tissue deformation is reduced. Thus, vibration-assisted needle insertion in general is expected to improve targeting accuracy. However, in order to generalize the proposed needle insertion technique, it is required to examine a wider range of vibration frequencies and amplitudes.

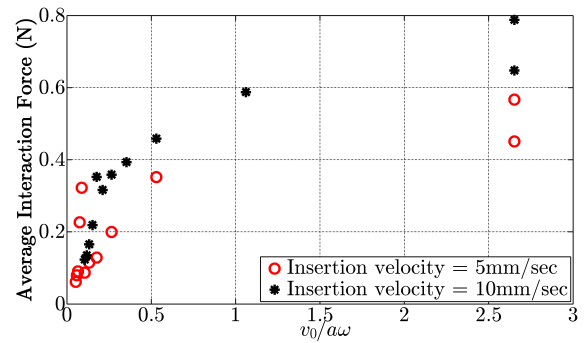


Fig. 9. Force magnitude versus velocity ratio ($\frac{v_0}{a\omega}$) of the vibrating needle.

Possible future extension includes investigating other types of *ex-vivo* soft tissue samples, e.g., liver, lung and bone. It is anticipated that the proposed technique will be particularly useful in bone biopsy where the dominant resistive force factor is Coulomb friction.

REFERENCES

- [1] N. Abolhassani, R. Patel, and M. Moallem, "Needle insertion into soft tissue: a survey," *Med. Eng. Phys.*, vol. 29, pp. 413–431, 2007.
- [2] A. Asadian, M.R. Kermani, and R.V. Patel, "A novel force modeling scheme for needle insertion using multiple Kalman filters," *IEEE Trans. Instrum. Meas.*, vol. 61, no. 2, pp. 429–438, 2012.
- [3] A.M. Okamura, C. Simone, and M.D. O'Leary, "Force modeling for needle insertion into soft tissue," *IEEE Trans. Biomed. Eng.*, vol. 51, no. 10, pp. 1707–1716, 2004.
- [4] M. Mahvash and P.E. Dupont, "Fast needle insertion to minimize tissue deformation and damage," *In Proc. of IEEE Int. Conf. on Rob. Autom. (ICRA)*, 2009, pp. 3097–3102.
- [5] D.J. Van Gerwen, J. Dankelman, and J.J. van den Dobbelsteen, "Needle–tissue interaction forces: A survey of experimental data," *Med. Eng. Phys.*, vol. 34, no. 6, pp. 665–680, 2012.
- [6] D. Minhas, J. Engh, M. Fenske, and C. Riviere, "Modeling of needle steering via duty-cycled spinning," *In Proc. of 29th IEEE EMBS Annu. Int. Conf. (EMBC)*, 2007, pp. 2756–2759.
- [7] T.K. Podder, D.P. Clark, D. Fuller, J. Sherman, W.S. Ng, L. Liao, D.J. Rubens, J.G. Strang, E.M. Messing, Y.D. Zhang, and Y. Yu, "Effects of velocity modulation during surgical needle insertion," *In Proc. of 27th IEEE EMBS Annu. Int. Conf.*, 2005, pp. 5766–5770.
- [8] T. Podder, "High frequency translational oscillation and rotational drilling of the needle in reducing target movement," *In Proc. of IEEE Int. Symp. on Comp. Intel. Rob. Aut. (CIRA)*, 2005, pp. 163–168.
- [9] N. Abolhassani, R. Patel, and M. Moallem, "Control of soft tissue deformation during robotic needle insertion," *Minimally Invasive Therapy & Allied Technologies*, vol. 15, pp. 165–76, 2006.
- [10] S. Badaan, D. Petrisor, C. Kim, and P. Mozer, "Does needle rotation improve lesion targeting?," *Int. J. Med. Robot. Comp.*, vol. 7, no. 2, pp. 138–147, 2011.
- [11] T. Shin-ei, K. Yuyama, M. Ujihara, and K. Mabuchi, "Reduction of insertion force of medical devices into biological tissues by vibration," *Japanese Journal of Medical Electronics and Biological Engineering*, vol. 39, pp. 292–296, 2001.
- [12] K. Muralidharan, "Mechanics of soft tissue penetration by a vibrating needle," University of Maryland, M.Sc. Thesis in Mechanical Engineering, 2007.
- [13] M.L. Mulvihill, D.E. Booth, and B.M. Park, "Medical tool for reduced penetration force," Aug. 31st, 2011, US Patent App. 13/222, 363.
- [14] C. Canudas De Wit, P. Tsiotras, E. Velenis, M. Basset, and G. Gissinger, "Dynamic friction models for road/tire longitudinal interaction," *Veh. Syst. Dyn.*, vol. 39, no. 3, pp. 189–226, 2003.
- [15] A. Asadian, R.V. Patel, and M.R. Kermani, "A distributed model for needle–tissue friction in percutaneous interventions," *In Proc. of IEEE Int. Conf. on Rob. Autom. (ICRA)*, 2011, pp. 1896–1901.
- [16] V.K. Astashev and V.I. Babitsky, "Ultrasonic processes and machines: dynamics, control and applications," Springer, 2007.